Toroidicity and shape dependence of peeling mode growth rates in axisymmetric toroidal plasmas*

Shi Bing-Ren(石秉仁)†

Southwestern Institute of Physics, Chengdu 610041, *China*

(Received 25 November 2013; revised manuscript received 7 January 2014; published online 28 May 2014)

The growth rate of the peeling mode instability with large toroidal mode number is calculated for general axisymmetric toroidal plasmas, including tokamaks and the spherical torus (ST) equilibia by using formalism presented by Connor *et al.* Analytic equilibia with non-zero edge current density and quasi-uniform current profiles are assumed. It is found that in sharp D-shape tokamak plasma, the derivative of the safety factor with respect to the poloidal flux becomes very large, making the perturbed poloidal motion very large, in turn making a significant reduction of the growth rate of the peeling mode, similar to the X-point effect in diverted plasma. The large aspect ratio effect is also studied, which reduces the growth rate further.

Keywords: peeling instability, D-shape and inverse D-shape configurations, todoidicity dependence

PACS: 52.55.Fa, 52.55.Rk **DOI:** 10.1088/1674-1056/23/7/075206

1. Introduction

Magnetohydrodynamic (MHD) instabilities in the tokamak pedestal region of the high-mode (H-mode) confinement are thought to be responsible for triggering the edge localized mode (ELMs) and understanding these instabilities is important for the control of the ELMs.[1] Responsible ideal MHD instabilities have been first studied widely both analytically[2–4] and numerically.[5–10] These are the peeling–ballooning type modes at intermediate toroidal mode number (∼3–30).[11–13] Analytical research[2–4] has been carried out for peeling modes with very large toroidal mode numbers for limiter configurations. For divertor configurations, some new developments appear recently[14–17] to treat the separatrix problem appropriately. Several non-ideal codes (NIMROD,[18] BOUT,[19,20] BOUT++,[21] M3D-C[22]) have been developed to include non-ideal effects, such as finite collisionality, ion diamagnetic stabilization, etc.

In recent years, numerical studies develop rapidly so that the peeling mode calculations can be routinely carried out. However, numerical studies usually assume particular equilibrium or directly use that determined by equilibrium codes. This makes it unfeasible to understand the parameter dependence of the mode growth rate on, such as the Toroidicity (the aspect ratio effect) or shaping effects. In this paper, we consider analytic equilibrium solution that covers the tokamak (its aspect ratio $R/a \approx 3$, with R being the major radius, a the half-width of the boundary at the mid-plane) and the spherical torus configurations (its aspect ratio $R/a \approx 1.2$) and also elongation and triangularity effects. The selected configurations are very similar to experimentally realized ones in many tokamak and ST devices. Some new phenomena are indicated. Especially, results for the typical D-shape configuration and the inverse D-shape (also called the negative triangularity) configuration are compared. Interest for the latter configuration is recently attracted due to its potentiality to alleviate the head load on the divertor plate of a tokamak reactor.

In Section 2, the formula of the growth rate of the peeling mode for general toroidally axisymmetric configuration is presented.[4,9] In Section 3 we introduce a Soloviev-type configuration. In Section 4, tokamak plasma is considered to analyze the shape effects. In Section 5, the spherical torus configuration is considered to analyze the aspect ratio effects on the growth rate of the peeling mode. In Section 6, a brief summary is made.

2. Growth rate of the peeling mode

The peeling mode instability of cylindrical plasma with non-zero edge current was first investigated in Ref. [2]. Such study was generalized to arbitrary toroidal plasma in Ref. [3] to obtain a general necessary stability condition that was widely used for analyzing the tokamak pedestal stability of the H regime. Later, Connor *et al.* re-derived this condition in a clearer way[4] that permits estimate of the growth rate of the unstable mode. To do this, we need to simultaneously determine the variations of potential energy and the kinetic energy.[9] In the following, we briefly introduce some basic formulae. A detailed description can be found in Ref. [23].

The growth rate γ of an unstable ideal MHD mode can be calculated from the energy principle as

$$\gamma^2 = \frac{-\delta W}{\int \mathrm{d}\tau \rho_0 |\boldsymbol{\xi}|^2}. \tag{1}$$

*Project supported by the National Magnetic Confinement Fusion Science Program of China (Grant No. 2009GB101002).

†Corresponding author. E-mail: shibr@swip.ac.cn

© 2014 Chinese Physical Society and IOP Publishing Ltd

For toroidally axisymmetric equilibrium, using an orthogonal coordinates $\boldsymbol{e}_\psi$, $\boldsymbol{e}_\varphi$, $\boldsymbol{e}_\zeta$, with ψ being the poloidal magnetic flux function, χ and ζ the poloidal and the toroidal angle-like variable, three components of the plasma displacement $\boldsymbol{\xi}(\boldsymbol{r},t)=\boldsymbol{\xi}(\psi,\chi)\,\mathrm{e}^{\gamma t-\mathrm{i}n\zeta}$ should be related by $\boldsymbol{\nabla}\cdot\boldsymbol{\xi}=0$ and $\boldsymbol{B}_0\cdot\boldsymbol{\xi}=B_\chi\xi_\chi+B_\zeta\xi_\zeta=0$, so that we have $|\boldsymbol{\xi}|^2=\xi_\psi^2+(1+B_\chi^2/B_\zeta^2)\xi_\chi^2$. Let $X=RB_\chi\xi_\psi$,[4] we use a formalism developed in Ref. [4] to consider large toroidal mode number n and assume the mode is localized around a rational mode surface where $q(\psi_0)=m/n$ and uniform along the field of lines as

$$X=\xi(\psi)\exp\left[-\mathrm{i}n\left(\zeta-\int^{\chi}\nu\,\mathrm{d}\chi'\right)\right], \tag{2}$$

with $\nu=IJ/R^2$ being the local pitch of the field line, and J the Jacobian. Using the localization condition, from $\boldsymbol{\nabla}\cdot\boldsymbol{\xi}=0$ we obtain

$$\xi_\chi=\frac{\mathrm{i}R^2B_\chi}{nI}\frac{\partial X}{\partial\psi}. \tag{3}$$

Finally, the unknown function $X(x)$ should be determined by minimization of the potential energy[3,4]

$$\delta W=\frac{\varepsilon^3}{2}\int\mathrm{d}x\left\{Px^2\left(\frac{\mathrm{d}\xi}{\mathrm{d}x}\right)^2+Q\xi^2+S\frac{\mathrm{d}}{\mathrm{d}x}(x\xi^2)\right\}. \tag{4}$$

Here we use the same terminologies as those in Ref. [4] and

$$P=2\pi q'^2\Big/\oint\frac{JB^2\mathrm{d}\chi}{R^2B_\chi^2}, \tag{5}$$

$$Q=\frac{p'}{2\pi}\oint\frac{\partial J}{\partial\psi}\mathrm{d}\chi-\frac{p'^2}{2\pi}\oint\frac{J\mathrm{d}\varphi}{B_\chi^2}+Ip'\oint\frac{J\mathrm{d}\varphi}{R^2B_\chi^2}\times\left[\frac{Ip'}{2\pi}\oint\frac{J\mathrm{d}\chi}{R^2B_\chi^2}-q'\right]\Big/\oint\frac{JB^2\mathrm{d}\chi}{R^2B_\chi^2}, \tag{6}$$

$$S=P+q'\oint\frac{j_{//}BJ\mathrm{d}\chi}{R^2B_\chi^2}\Big/\oint\frac{JB^2\mathrm{d}\chi}{R^2B_\chi^2}. \tag{7}$$

The corresponding Euler equation is

$$\frac{\mathrm{d}}{\mathrm{d}x}\left(x^2\frac{\mathrm{d}\xi}{\mathrm{d}x}\right)-\frac{Q}{P}\xi=0. \tag{8}$$

Around the singular layer, Q and P can be treated as constants, leading to the Mercier-like solutions[4]

$$\xi=a_+x^{\lambda_+}+a_-x^{\lambda_-}, \tag{9}$$

where

$$\lambda_\pm=-\frac{1}{2}\pm\sqrt{\frac{1}{4}+\frac{Q}{P}}. \tag{10}$$

Quantity $Q/P=-D_\mathrm{M}$ is the Mercier coefficient.[25] The solutions (9) mean that the eigen-functions only depend on the Mercier coefficient and the presence of the edge current does not affect these functions. Now we are interested in the situation where the rational surface is outside the plasma. Assuming that the location of the rational surface is at $x=0$ while the plasma boundary is at $x=\Delta>0$, inside the plasma $\Delta<x<\infty$, then we obtain after substituting Eq. (9) into Eq. (4)

$$\delta W=-\frac{\varepsilon^3}{2}a_-^2P\Delta^{2\lambda_-+1}\left[\lambda_-+\frac{S}{P}\right]. \tag{11}$$

The above derivation also gives the displacement components of interest

$$\xi_\psi=X/RB_\chi=a_-x^{\lambda_-}/RB_\chi, \tag{12}$$

$$\xi_\chi=\mathrm{i}a_-\left(\frac{R^2B_\chi\lambda_-}{nI}\right)x^{\lambda_--1}. \tag{13}$$

Using these results, for the kinetic energy we obtain

$$K=\pi\varepsilon^3a_-^2\rho_0\left[\left(\oint\frac{J\mathrm{d}\chi}{R^2B_\chi^2}\right)\frac{\Delta^{2\lambda_-+1}}{2\lambda_-+1}+\left(\oint\frac{R^4B_\chi^2}{I^2}J\mathrm{d}\chi\right)\frac{\Delta^{2\lambda_--1}}{n^2(2\lambda_--1)}\right]. \tag{14}$$

The growth rate can be determined by

$$\gamma^2=\frac{1}{2\pi\rho_0}\frac{\lambda_-P+S}{A}, \tag{15}$$

$$A=-\frac{1}{2\lambda_-+1}\oint\frac{J\mathrm{d}\chi}{R^2B_\chi^2}-\frac{\lambda_-^2}{n^2\Delta^2(2\lambda_--1)I^2}\oint R^4B_\chi^2J\mathrm{d}\chi. \tag{16}$$

Assuming that $q_\mathrm{s}=m/n$ and $q_\mathrm{a}=m/n+q'(\psi)(\psi_0-\psi_\mathrm{a})$, then we have

$$\Delta=\frac{\psi_0-\psi_\mathrm{a}}{\varepsilon}=\frac{(m/n-q_\mathrm{a})}{q'\varepsilon}, \tag{17}$$

$$\frac{1}{n\Delta}=\frac{q'\varepsilon}{(m-nq_\mathrm{a})}. \tag{18}$$

We are interested in case of $q'\varepsilon\approx1$ and $0\le m-nq_\mathrm{a}\le1$. Using the above results, the kinetic term becomes

$$K=\pi\varepsilon^3\rho_0\xi_0^2\Delta^{2\lambda_-+1}\left[\frac{1}{|2\lambda_-+1|}\oint\frac{J\mathrm{d}\chi}{|\nabla\psi|^2}+\frac{\lambda_-^2}{|2\lambda_--1|}\frac{q'^2}{F^2}\oint R^4B_\chi^2J\mathrm{d}\chi\right]. \tag{19}$$

Defining $\omega_\mathrm{A}^2=B^2/\rho_0R_0^2$, the general expression of the growth rate becomes

$$(\gamma^2/\omega_\mathrm{A}^2)=\frac{(\lambda_-+1)+\oint jBJ\mathrm{d}\chi/2\pi q'|\nabla\psi|^2}{(B/R_0)^2\oint B^2J\mathrm{d}\chi[(1/|2\lambda_-+1|)\oint J\mathrm{d}\chi/q'^2|\nabla\psi|^2+(\lambda_-^2/F^2)\oint R^4B_\chi^2J\mathrm{d}\chi]/|\nabla\psi|^2}. \tag{20}$$

3. Soloviev-type configuration[24,26,27]

To simulate a tokamak pedestal region, we use the simple Soloviev-type equilibrium of up–down symmetry, and assume the following type solution of the Grad-Shafranov equation:

$$\psi = \frac{\psi_b}{y_b^2}\left[\frac{4}{E^2}(1+(1-D)y)\frac{z^2}{R_0^2}+y^2\right], \tag{21}$$

$$y = \frac{R^2}{R_0^2}-1. \tag{22}$$

In above solution, subscript "b" means the boundary, and parameter E corresponds to the elongation of the cross-section, while D is related to the triangularity of a D-shape configuration. Introduce flux-based new variable

$$y_\psi = y_b\sqrt{\psi/\psi_b}, \tag{23}$$

and a poloidal angle-like variable u from the transformations

$$\begin{aligned} R &= R_0\sqrt{1+y_\psi\cos u} = R_0\sqrt{f_1}, \\ z &= \frac{ER_0}{2}\frac{y_\psi\sin u}{\sqrt{1+(1-D)y_\psi\cos u}} = \frac{ER_0 y_\psi\sin u}{2\sqrt{f_2}}. \end{aligned} \tag{24}$$

Thus, we have

$$\frac{\partial\psi}{\partial R} = \frac{4\psi_b y_\psi\sqrt{f_1}f_3}{y_b^2R_0}, \tag{25}$$

$$\frac{\partial\psi}{\partial z} = \frac{4\psi_b y_\psi}{y_b^2R_0}\frac{\sqrt{f_2}\sin u}{E}, \tag{26}$$

$$|\nabla\psi| = \frac{4\psi_b y_\psi}{y_b^2R_0}\sqrt{f_4} = \frac{EI(0)}{2q_0}(y_\psi\sqrt{f_4}), \tag{27}$$

where

$$f_1 = 1+y_\psi\cos u, \tag{28}$$

$$f_2 = 1+(1-D)y_\psi\cos u, \tag{29}$$

$$f_3 = \cos u+(1-D)y_\psi\sin^2 u/2f_2, \tag{30}$$

$$f_4 = f_1f_3^2+f_2\sin^2 u/E^2, \tag{31}$$

and the Jacobian

$$J = \left(\frac{8\psi_b}{y_b^2ER_0^3}\right)\sqrt{f_2})^{-1} = \frac{y_b^2ER_0^3}{8\psi_b\sqrt{f_2}}. \tag{32}$$

Using $J\,\mathrm{d}u = \mathrm{d}l/B_\chi$, integrals in above sections can be directly calculated. Especially, the safety factor q and its derivative with respect to ψ can be expressed by

$$\begin{aligned} q(\psi) &= \frac{I}{2\pi}\oint\frac{J\,\mathrm{d}\chi}{R^2} \\ &= \frac{y_b^2IER_0}{8\pi\psi_b}\int_0^\pi\frac{\mathrm{d}u}{f_1\sqrt{f_2}} \\ &= \frac{q_0I}{\pi I(0)}\int_0^\pi\frac{\mathrm{d}u}{f_1\sqrt{f_2}}, \end{aligned} \tag{33}$$

$$\begin{aligned} q'(\psi) &= I'q/I-\frac{y_b^3EIR_0}{16\pi\psi_b^{3/2}\sqrt{\psi}}\int_0^\pi\mathrm{d}u\frac{(\cos u-f_5\sin^2 u)}{f_1\sqrt{f_2}} \\ &\quad\times\left(\frac{1}{f_1}+\frac{1-D}{2f_2}\right). \end{aligned} \tag{34}$$

The value of $q'(\psi)$ can also be calculated by direct derivative.

4. Tokamak plasmas

For tokamak plasma, the quantity $I = RB_\zeta$ can be approximately taken as constant. Set $y_b = 0.625$ and $E = 1.6$, by changing parameter D, different plasma boundary can be obtained. We are mainly interested in configurations with D-shape boundary. For comparison, we consider two D-shape configurations, one has inner D-shape (the routinely used by general tokamas), the other has outward D-shape (the inverse D-shape). Both have almost straight boundary in inner or outward side, as shown in Fig. 1 (the latter is also called the negative triangularity configuration). Relationship of the parameter D with the triangularity can be found in Ref. [24].

It is found that all surface quantities in Eqs. (6)–(7) and (19) are sensitive to the Jacobian and the value of $|\nabla\psi|$. As an example, we consider the variation of $|\nabla\psi|$ along the poloidal direction. For D-shape configurations with sharp boundary, this value exhibits a sharp decrease in very local region (near the inner mid-plane for D-shape or near the external mid-plane for the inverse D-shape) while for elliptic boundary, its variation is relatively small, as shown in Fig. 2.

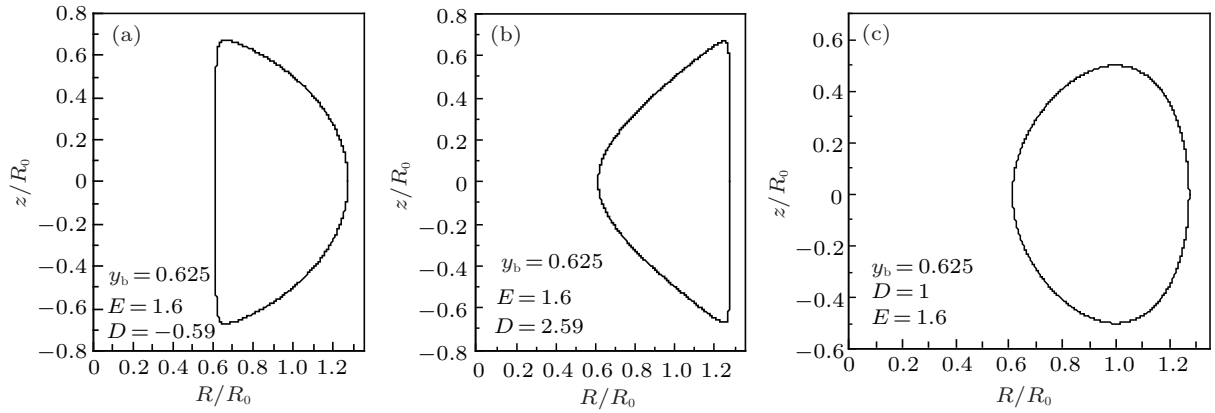


Fig. 1. Examples of tokamak boundary. (a) Boundary with D-shape; (b) boundary with inverse D-shape; and (c) elliptic boundary.

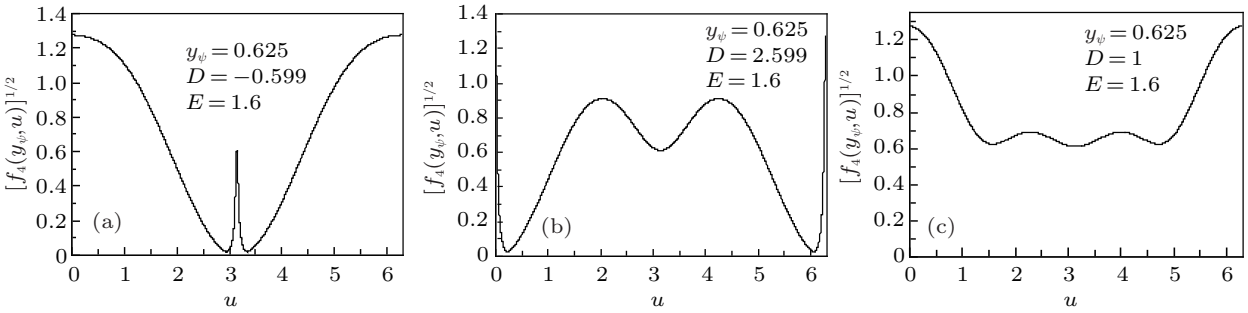


Fig. 2. Variation of $|\nabla\psi|$ along the poloidal boundary for configurations shown in Fig. 1. (a) D-shape; (b) inverse D-shape; and (c) elliptic.

4.1. The Mercier index

To calculate the Mercier index, $D_{\rm M} = -Q/P$, we first rewrite the relevant quantities as

$$\bar{Q} = Q \oint \frac{JB^2 {\rm d}\chi}{|\nabla\psi|^2} = p' M_1 + p'^2 M_2, \tag{35}$$

$$D_{\rm M} = -\bar{Q}/2\pi q'^2, \tag{36}$$

$$M_1 = \frac{1}{2\pi}\left(\frac{\partial}{\partial\psi}\oint J{\rm d}\chi\right)\left(\oint \frac{JB^2{\rm d}\chi}{|\nabla\psi|^2}\right) - Iq'\oint\frac{J{\rm d}\chi}{|\nabla\psi|^2}, \tag{37}$$

$$M_2 = \frac{I^2}{2\pi}\left(\oint\frac{J{\rm d}\chi}{|\nabla\psi|^2}\right)^2 - \frac{1}{2\pi}\left(\oint\frac{R^2 J{\rm d}\chi}{|\nabla\psi|^2}\right) \times \left(\oint\frac{B^2 J{\rm d}\chi}{|\nabla\psi|^2}\right). \tag{38}$$

Using these relations, we obtain

$$-p'M_1/2\pi q'^2 = \frac{E^2+1-D}{E^2 y_{\rm b}}\left(\frac{\psi_{\rm b}}{\psi}\right)^{1/2}\left[I_4\left(\frac{\partial}{\partial y_\psi}\int\frac{{\rm d}u}{\sqrt{f_2}}\right)\Big/\left(\frac{\partial}{\partial y_\psi}\int\frac{{\rm d}u}{f_1\sqrt{f_2}}\right) - I_5\right]\Big/\left(\frac{\partial}{\partial y_\psi}\int\frac{{\rm d}u}{f_1\sqrt{f_2}}\right), \tag{39}$$

$$-p'^2M_2/2\pi q'^2 = \left(\frac{E^2+1-D}{E^2 y_{\rm b}}\right)^2\left(\frac{\psi_{\rm b}}{\psi}\right)\frac{\left[\left(\int {\rm d}u/f_4\sqrt{f_2}\right)^2 - \left(\int f_1\,{\rm d}u/f_4\sqrt{f_2}\right)\left(\int {\rm d}u/f_1 f_4\sqrt{f_2}\right)\right]}{\left((\partial/\partial y_\psi)\int {\rm d}u/f_1\sqrt{f_2}\right)^2}, \tag{40}$$

$$D_{\rm M} = c_{\rm M}\{[I_4 I_{\rm VP}/I_{\rm qp} - I_5]/I_{\rm qp} + c_{\rm M}[I_5^2 - I_4 I_6]/I_{\rm qp}^2\}, \tag{41}$$

$$c_{\rm M} = \left(\frac{E^2+1-D}{E^2 y_{\rm b}}\right)\left(\frac{\psi_{\rm b}}{\psi}\right)^{1/2}. \tag{42}$$

In the above equations, we define several integrals as

$$I_1 = \frac{1}{\pi}\int_0^\pi \frac{{\rm d}u}{f_1\sqrt{f_2}},\quad I_2 = \int_0^\pi \frac{\cos u\,{\rm d}u}{f_2^{3/2}},$$

$$I_3 = \int_0^\pi {\rm d}u\frac{\cos u}{f_1\sqrt{f_2}}\left(\frac{1}{f_1} + \frac{1-D}{2f_2}\right),$$

$$I_{\rm VP} = \frac{\partial}{\partial y_\xi}\int_0^\pi\frac{{\rm d}u}{\sqrt{f_2}},\quad I_{\rm qp} = \frac{\partial}{\partial y_\psi}\int_0^\pi\frac{{\rm d}u}{f_1\sqrt{f_2}},$$

$$I_4 = \int_0^\pi\frac{{\rm d}u}{f_1 f_4\sqrt{f_2}},\quad I_5 = \int_0^\pi\frac{{\rm d}u}{f_4\sqrt{f_2}},$$

$$I_6 = \int_0^\pi\frac{f_1\,{\rm d}u}{f_4\sqrt{f_2}},\quad I_J = \int_0^\pi {\rm d}u f_1 f_4/\sqrt{f_2}.$$

In these results, we use the self-consistent equilibrium relations about the $p'(\psi)$ and $I'^2(\psi)$. For the peeling mode analysis, we are interested in the stable Mercier mode, i.e., $D_{\rm M} < 1/2$. It is found that the Mercier index is in the stable regime, denoting the first part and the second part of the right-hand side of Eq. (31) as $D_{\rm M1}$ and $D_{\rm M2}$. The variations of these two parts and their sum, $D_{\rm M} = D_{\rm M1} + D_{\rm M2}$, with the change of the triangularity parameter D is shown in Fig. 3.

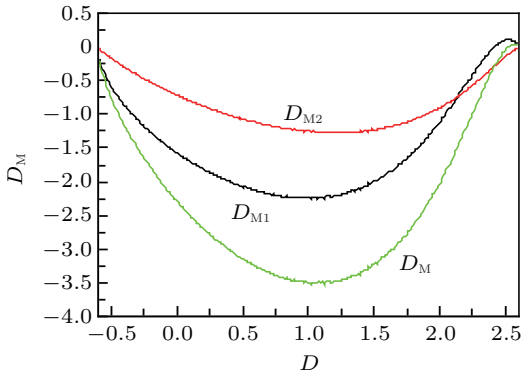


Fig. 3. (color online) The Mercier index $D_{\rm M}$ versus the triangularity parameter D for $y_{\rm b} = 0.625$ and $E = 1.6$.

4.2. Current driven term

The edge localized peeling mode is basically driven by the non-zero edge current.[1–4] The contribution of this term to the variation of the potential energy is expressed by $\mu_0\oint(\boldsymbol{j}\cdot$

$BJ\,\mathrm{d}\chi/|\nabla\psi|^2)/\pi q'$. Using the equilibrium relation, we have

$$\mu_0 jB \approx \mu_0 j_\zeta B_\zeta = \left(-p' - \frac{I'^2}{2R^2}\right) I, \tag{43}$$

$$\mu_0 \oint \frac{jBJ\,\mathrm{d}\chi}{|\nabla\psi|^2} = -\mu_0 I p' \oint \frac{J\,\mathrm{d}\chi}{|\nabla\psi|^2} - \frac{II'^2}{2} \oint \frac{J\,\mathrm{d}\chi}{R^2|\nabla\psi|^2}. \tag{44}$$

Then, using the following relationships:[24]

$$\mu_0 p' = -\mu_0 p_0/\psi_\mathrm{b} = -\frac{8\psi_\mathrm{b}(E^2+1-D)}{y_\mathrm{b}^2 E^2 R_0^4}, \tag{45}$$

$$I'^2/2 = I_1^2/\psi_\mathrm{b} = -\frac{8D\psi_\mathrm{b}}{y_\mathrm{b}^2 E^2 R_0^2}, \tag{46}$$

$$\mu_0 R j_\zeta = \left(\frac{8\psi_\mathrm{b}}{y_\mathrm{b}^2 E^2 R_0^2}\right)\left[(E^2+1-D)\left(\frac{R}{R_0}\right)^2 + D\right], \tag{47}$$

we obtain

$$\mu_0 R j_\zeta = \left(\frac{8\psi_\mathrm{b}}{y_\mathrm{b}^2 E^2 R_0^2}\right)\left[(E^2+1-D)\left(\frac{R}{R_0}\right)^2 + D\right], \tag{48}$$

$$\begin{aligned}&\mu_0 \oint \frac{jBJ\,\mathrm{d}\chi}{|\nabla\psi|^2}/(\pi q') \\ &= \left(\frac{1}{\pi E^2 y_\psi}\right)\left[(E^2+1-D)\int_0^\pi \frac{\mathrm{d}u}{f_4\sqrt{f_2}} + D\int_0^\pi \frac{\mathrm{d}u}{f_1 f_4\sqrt{f_2}}\right] \\ &\Big/ \left(\frac{\partial}{\partial y_\psi}\frac{1}{\pi}\int_0^\pi \frac{\mathrm{d}u}{f_1\sqrt{f_2}}\right).\end{aligned} \tag{49}$$

If we denote this term as $-\delta W_\mathrm{JB}$ and define $-\delta W = -[(\lambda_- + 1) + \delta W_\mathrm{JB}]$, the variation of the potential energy will be proportional to $-\delta W$. The variation of these two quantities with the triangularity parameter D is shown in Fig. 4.

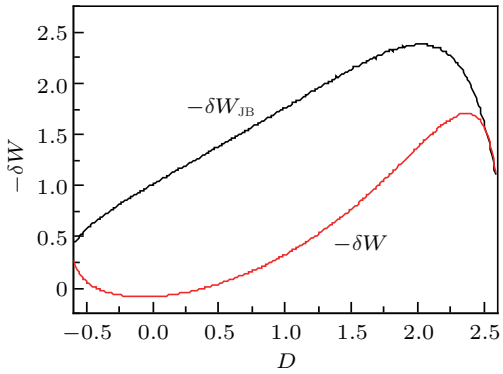


Fig. 4. (color online) Variation of the total potential energy with D for $y_\mathrm{b} = 0.625, E = 1.6$. The contribution from the current driven term is also indicated.

4.3. Distributions of $|\xi_\psi|^2$ and $|\xi_\chi|^2$ along the poloidal angle[9]

An important feature of the peeling mode is the quite different distribution of the normal component of the displacement function from its poloidal component along the poloidal angle. We now determine their contributions to the variation of the kinetic energy. From the expression of the kinetic energy variation (Eq. (19)), we can find that contribution from the normal component of the displacement, $|\xi_\psi|^2$, can be written as $CJ/|\nabla\psi|^2 \propto A/f_4\sqrt{f_2}$, while that from the poloidal component is

$$\begin{aligned}|\xi_\chi|^2 &= [(C/3)q'^2/F^2]R^4 B_\chi^2 J \propto A(E^2 y_\mathrm{p}^2/3\pi^2) \\ &\times \left(\frac{\partial}{\partial y_\psi}\int_0^\pi \frac{\mathrm{d}u}{f_1\sqrt{f_2}}\right)^2 f_1 f_4/\sqrt{f_2}.\end{aligned} \tag{50}$$

To plot $\sqrt{|\xi_\psi|^2}$ and $\sqrt{|\xi_\chi|^2}$ as functions of the poloidal variable u, for a D-shape plasma, we find that, with the inner boundary getting much steeper (the parameter $y_\psi \to 0.625$), the poloidal component becomes much greater than the normal component and much localized (Figs. 5(a) and 5(b)) while for the inverse D-shape case, if the magnetic shear is not large, two components could be comparable (Fig. 5(c)).

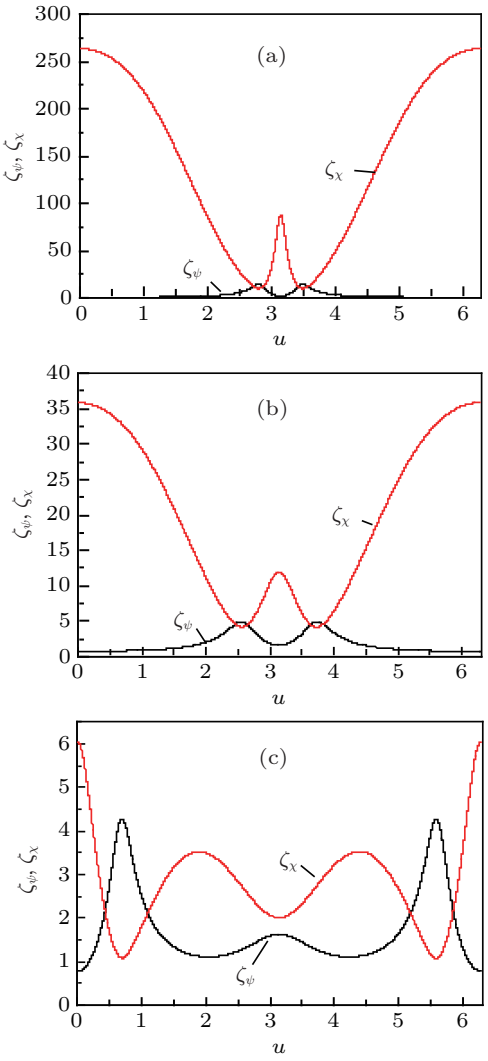


Fig. 5. (color online) Displacement functions along the poloidal direction for different boundary parameters: (a) $y_\psi = 0.625$, $E = 1.6$, $D = -0.59$, (b) $y_\psi = 0.625$, $E = 1.6$, $D = -0.5$, and (c) $y_\psi = 0.625$, $E = 1.6$, $D = 2.5$.

4.4. Growth rate of the peeling mode

Now we can use the general equation, $\gamma^2 = -\delta W/K$, to calculate the growth rate of edge peeling mode for an arbitrary D-shape Solov'ev configuration described above. Using results described in above sections, we can finally write

$$(\gamma^2/\omega_{\rm A}^2) = \frac{(\lambda_- + 1) + (2\pi E^2 y_\psi)^{-1}[(E^2+1-D)I_5 + DI_4]/I_{\rm pq}}{q_0^2[(E^2 y_\psi^2)^{-1} I_5/I_{\rm pq}^2 + I_J]I_4}. \quad (51)$$

For simplicity, in the following we denote $\gamma^2 q_0^2/\omega_{\rm A}^2 \Rightarrow \gamma^2$ as a normalized quantity (the square of normalized growth rate). Including two D-shape configurations, the general variation of the square of the growth rate of the edge peeling mode in such kind of Solov'ev configuration is shown in Fig. 6. It is found that in parameter range $-0.41 \le D < -0.11$, $\gamma^2 < 0$, the mode is stable. For D-shape case, with $D < -0.41$, the growth rate is small while in the inverse D-shape case, the growth rate is usually much greater than in the D-shape case. However, when the parameter $D > 2.5$, i.e., when the outer boundary becomes rather straight, the growth rate rapidly decreases. The basic reason that the growth rate becomes very small in both of these two limiting cases is not due to the decrease of the variation of the potential energy (indeed, these variations are increasing), but due to the rapid increase of the poloidal displacement value. This situation is quite similar to the case of a diverted plasma when the very near separatrix surface is approached.[1,14–17]

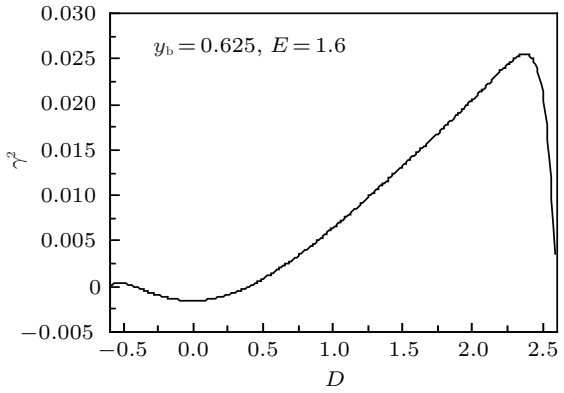


Fig. 6. Variation of the square of the normalized growth rate of the edge peeling mode, γ^2, with the triangularity parameter D.

5. Spherical torus configuration

Analyses carried out above indicate that the magnetic shear in the tokamak edge (due to large $q'(\psi)$) has significant effects on the edge peeling mode. It is undoubtedly very interesting to consider the large aspect ratio case, the spherical torus configuration, because it has a large magnetic shear in its edge region naturally.[24] Now assume a configuration with aspect ratio $A = 1.2$ and $E = 1.6$, which is equivalent to $y_{\rm b} = 2A/(A^2+1) = 0.9836$. Examples of the boundary of this kind of configurations are shown in Fig. 7. Using the same method as the one discussed above for tokamaks, we obtain the Mercier index in Fig. 8. It is apparent that dominant effect is from the $D_{\rm M1}$ term, producing a quite strong stabilizing effect. Then for typical D-shape ST configuration, the current driving term is smaller than the Mercier term, so that the edge peeling mode is stable. This happens for $D < 0.129$ (Fig. 9) while the absolute value of λ_- becomes larger than the absolute value of S/P so that the total variation of the potential energy is positive.

Even in the unstable parameter regime, the absolute value of the displacement function becomes very large and usually the poloidal displacement is much larger than the normal one by several orders. This makes γ^2 much smaller than the tokamak case (Fig. 10).

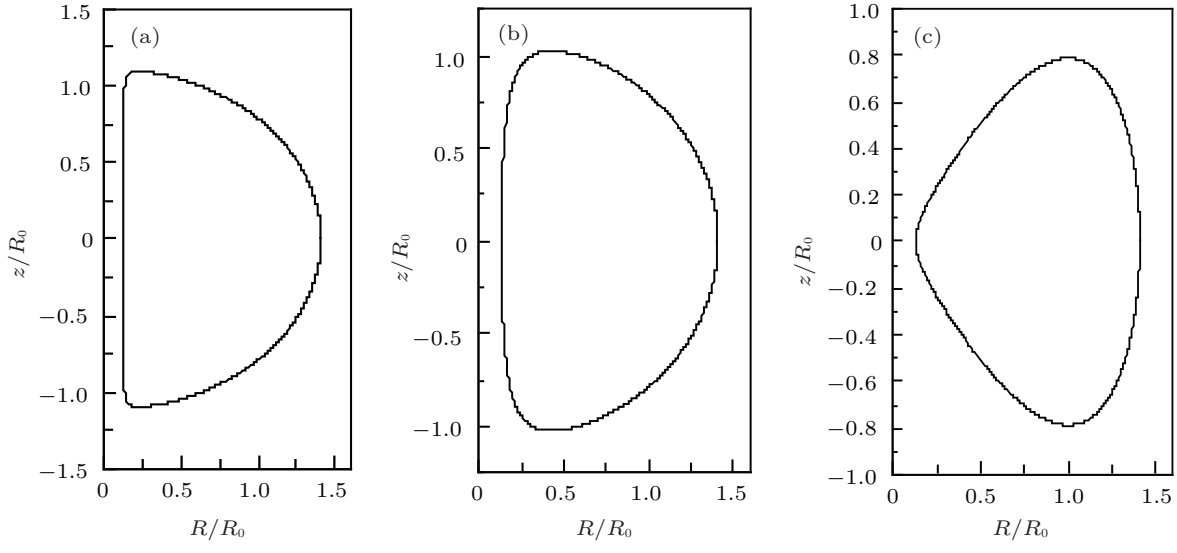


Fig. 7. Boundary of an ST configuration with $y_{\rm b} = 0.9836$, and $E = 1.6$. (a) $D = -0.016$, (b) $D = 0$, and (c) $D = 1.0$.

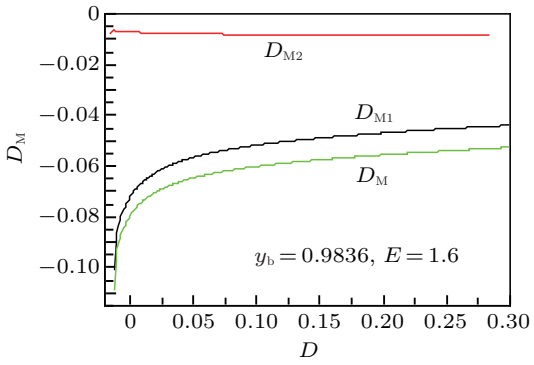


Fig. 8. (color online) Variation of the Mercier index D_M of the ST configuration with parameter D.

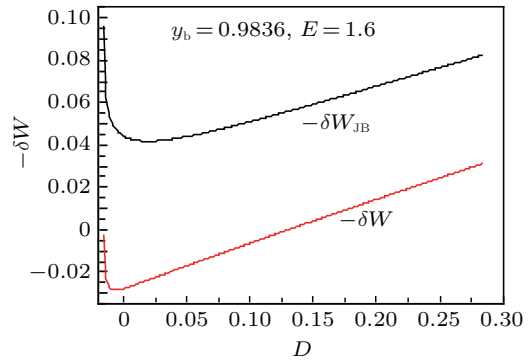


Fig. 9. (color online) Change of the total variation of the potential energy, $-\delta W$ for the ST configuration with parameter D.

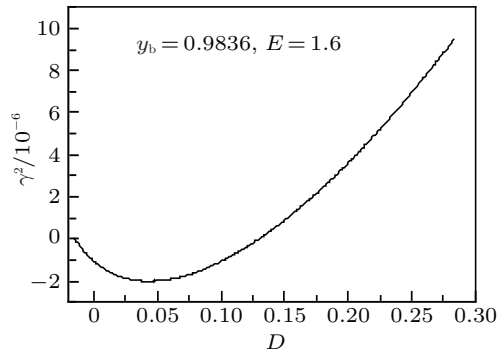


Fig. 10. Change of the square of the growth rate γ^2 for the ST configuration with parameter D.

6. Summary

We have calculated the growth rate of the edge peeling mode for the tokamak and the ST configurations. For tokamaks, results are compared for regular D-shape and inverse D-shape cases. Generally, the variation of the kinetic energy is dominated by the perturbed poloidal displacement, which becomes very large in a large magnetic shear region. This makes the growth rate of the peeling mode very small in near D-shape and also the inverse D-shape boundary. This situation is somewhat similar to the case of diverted plasma when the separatrix is approached. Of course, this is only a simple one-dimensional analysis, so it would be interesting if a more complicated numerical simulation could find similar results.

References

[1] Webster A J 2012 *Nucl. Fusion* **52** 114023
[2] Laval G, Pellat R and Soule J S 1974 *Phys. Fluids* **17** 835
[3] Lortz D 1975 *Nucl. Fusion* **15** 49
[4] Connor J W, Hastie R J, Wilson H R and Miller R L 1998 *Phys. Plasmas* **5** 2687
[5] Medevedev S Y, Martynov A A, Matin Y R, Sauter O and Villard L 2006 *Plasma Phys. Contr. Fusion* **48** 927
[6] Huysmans G T A 2005 *Plasma Phys. Contr. Fusion* **47** 2107
[7] Huysmans G T A and Czarny O 2007 *Nucl. Fusion* **47** 659
[8] Saarelma S, Alfier A, Beuskans M N A, Coelho R, Koslowski H R, Liang Y, Nunes I and JET EFDA Contributors 2009 *Plasma Phys. Contr. Fusion* **51** 035001
[9] Wilson H R, Snyder P B, Husmans G T A and Miller R L 2002 *Phys. Plasmas* **9** 1277
[10] Ferraro N M, Jardin S C and Snyder P B 2010 *Phys. Plasmas* **17** 102508
[11] Snyder P B, Wilson H R, Ferron J R, Lao L L, Leonard A W, Osborne T H, Turnbull A D, Mossessian D, Murakami M and Xu X Q 2002 *Phys. Plasmas* **9** 2037
[12] Huysmans G T A 2005 *Plasma Phys. Contr. Fusion* **47** B165
[13] Wilson H R, Cowley S C, Kirk A and Snyder P B 2006 *Plasma Phys. Contr. Fusion* **48** A71
[14] Webster A J 2009 *Phys. Plasmas* **16** 012501
[15] Webster A J and Gimblett C G 2009 *Phys. Rev. Lett.* **102** 035003
[16] Webster A J and Gimblett C G 2009 *Phys. Plasmas* **16** 082502
[17] Webster A J 2009 *Phys. Plasmas* **16** 082503
[18] Burke B J, Kruger S E, Hegna C C, Zhu P, Snyder P B, Sovinec C R and Howell E C 2010 *Phys. Plasmas* **17** 032103
[19] Xu X Q, Cohen R H, Nevins W M, Porter G D, Rensink M E, Rognlien T D, Myra J R, Dlppolito D A, Moyer R A, Snyder P B and Cartstrom T N 2002 *Nucl. Fusion* **42** 21
[20] Snyder P B, Wilson H R and Xu X Q 2005 *Phys. Plasmas* **12** 056115
[21] Dudson B D, Umanski M V, Xu X Q, Snyder P B and Wilson H R 2009 *Comput. Phys. Commun.* **180** 1467
[22] Federici G, Loarte A and Strohmayer G 2003 *Plasma Phys. Contr. Fusion* **45** 1523
[23] Shi B R 2014 *Chin. Phys. B* **23** 015202
[24] Shi B R 2004 *Plasma Phys. Contr. Fusion* **46** 1105
[25] Mercier C 1960 *Nucl. Fusion* **1** 47
[26] Wening R H 1997 *Phys. Plasmas* **4** 3254
[27] Wening R H 2000 *Phys. Plasmas* **7** 3654